Comparison of a finite element model with a mutliple-scales solution for sound propagation in varying ducts with swirling flows

Fabien Treyssède, Mabrouk Ben Tahar

Comparison of a finite element model with a mutliple-scales solution for sound propagation in varying ducts with swirling flows

Fabien Treyssède[a)], and Mabrouk Ben Tahar

Université de Technologie de Compiègne, Laboratoire Roberval UMR 6066,

Secteur Acoustique, BP 20529, 60205 Compiègne Cedex, FRANCE

Received:

Suggested running title: "Sound propagation in ducted swirling flows"

[a)]Electronic mail: fabien.treyssede@utc.fr

Abstract:

A multiple-scales (MS) solution is proposed to study sound propagation in slowly varying ducts with mean swirling flows. Instead of the standard linearized Euler equations, the MS method is applied to the so-called Galbrun's equation. This equation is based on an Eulerian-Lagrangian description and corresponds to a wave equation written only in terms of the Lagrangian perturbation of the displacement. This yields simpler differential equations to solve for the MS model as well as simpler boundary conditions. In this paper, Galbrun's equation is also solved by a mixed pressure-displacement finite element method (FEM). The proposed FEM model has already been tested in authors' previous papers. This model is quite general and is extended here to arbitrary mean flows, including compressibility and swirling flow effects. Some MS and FEM solutions are then compared in order to validate both models.

PACS numbers: 43.20.Bi, 43.28.Py, 43.20.Mv

LIST OF SYMBOLS

$D, C, P, \mathbf{V}$	mean flow variables
$p, \mathbf{w}$	acoustic variables
ω	pulsation
$d(\cdot)/dt$	material derivative
(r,θ,z)	cylindrical coordinates
$\mathbf{n}$	outward normal
Z_1, Z_2	inner and outer wall impedances
R_1, R_2	inner and outer duct radii
$Z = \varepsilon z$	slow axial scale
k_z	local axial wave number
m	azimuthal mode number
$D_0, C_0, P_0, \mathbf{V_0}$	0^{th} order mean flow variables
$p_0, \mathbf{w_0}$	0^{th} order acoustic variables
Ω	flow modified pulsation
$L, L^\dagger$	acoustic operator and its adjoint
$\psi_0, \psi_0^\dagger$	0^{th} order eigenfunction and its adjoint
Ω_a	fluid domain
Γ_i	wall boundary
Γ_w	forced displacement boundary

$p^*, \mathbf{w}^*$	trial fields
L^*, C^*	characteristic length and sound speed
M_0, Ω_0	axial and azimuthal Mach number
$\overline{\mathbf{i}}$	time-averaged intensity ($\mathrm{W.m^{-2}}$)
μ	total duct attenuation (dB)

I. INTRODUCTION

Mean swirling flows may have a significant impact upon sound propagation in ducts, particularly when turbomachines are involved. For instance, the fan of an aeroengine duct is likely to generate a significant rotating flow, for which the azimuthal velocity can even be comparable to the axial component. It is then obvious that the effects of swirl on acoustic wave propagation cannot be neglected.

Almost all analyses taking into account such effects deal with the study of a mode propagating inside a simple straight duct[1,2,3,4,5]. This work has notably provided a meaningful understanding of coupling that occurs between the so-called acoustic and rotational waves.

Recently, Cooper and Peake[6] extended Golubev and Atassi's study[4] to slowly varying lined ducts by applying a multiple-scales (MS) method. Results outlined the influence of mean flow swirl, which produces a large difference in axial wavenumber and moves co-rotating modes closer to cut-off (counter-rotating modes are moved further). One consequence is that, when a lining is present at walls, co-rotating modes are always much more damped than those in a non-swirling flow (counter-rotating modes may be amplified).

In order to describe sound propagation in swirling flows, all the above references are based on the linearized Euler equations (note that the standard full-potential equation, which assumes that both acoustics and aerodynamics are irrotational, cannot be considered). However, there exists another wave equation, the so-called Galbrun's equation[7] also derived by Godin[8], which is a reformulation of the linearized Euler equations using an Eulerian-Lagrangian description. Galbrun's equation constitutes a second-order partial differential equation, which has the particularity to be written only in terms of the Lagrangian perturbation of the displacement vector (itself expressed with Eulerian variables). Theoretical details about this equation are given in Refs. 8, 9.

Few works deal with this equation, but it may have the following several advantages: a gain of one to two unknowns compared to the linearized Euler equations, availability of exact expressions of intensity and energy[8,10], simple expressions of boundary conditions (compared to Myers' condition[11]). Studying a single mode propagating in a straight duct with swirling flows, Poirée[12] derived a differential equation from Galbrun's equation that is satisfied by the radial component of the Lagrangian displacement.

In this paper, a MS method based on Galbrun's equation is proposed to solve sound propagation in slowly varying lined ducts with swirling flows. The overall method is inspired from Rienstra's[13] and Cooper and Peake's[6] papers. The proposed model does not a priori provide some great insights from a physical point of view compared to

Cooper and Peake's, but equations are much easier to solve and the mean flow being considered is not necessarily homentropic (though no such flows are considered for the numerical results presented in this paper).

A second part of the paper consists in proposing a quite general finite element method (FEM) to solve Galbrun's equation in the harmonic case, for any arbitrary mean flow whether it is sheared, swirling or/and compressible. It has to be emphasized that some work has been made to solve the general linearized equations of fluid mechanics using a FEM. This work concerns the linearized Euler equations in the late 1970s[14,15,16], as well as Galbrun's equation more recently[10,17,18,19]. Unfortunately, the effects of swirling flows have not yet been specifically studied in those analyses.

Here, the proposed FEM is applicable to any type of flow. The choice of a mixed pressure-displacement variational formulation combined with a finite element satisfying the inf-sup condition avoids the well-known locking phenomenon, which usually occurs with a purely displacement based formulation. The developed FEM model has already been successfully tested in authors' recent papers for sound propagation in sheared flows[18] and vibro-acoustic interactions[19]. The slight difference with those references comes from the fact that the variational formulation is now quite general because it includes the additional terms inherent to mean flow compressibility effect, which were not previously considered.

The last part of the paper gives some numerical results in the axisymmetric case, obtained with the MS and FEM models. The main goal of this part is to validate both models and to verify that they adequately include the effects of swirl upon acoustic propagation.

II. MULTIPLE-SCALES SOLUTION FOR ACOUSTICS

This section only gives the multiple-scales solution for acoustics, based on Galbrun's equation. A multiple-scales solution for the mean flow has already been considered in Ref. 6 and will not be detailed here. More insight about Galbrun's equation can be found in Ref. 8, 9, 10 and 19.

The multiple-scales methodology (see for instance Refs. 20, 21 and 22) may be divided into three main parts. First, a slowly varying parameter is defined and used to rewrite governing equations. Secondly, a local eigenvalue problem is solved at each duct cross-section (0^{th} order solution). Thirdly, a solvability condition is derived from the first order problem in order to get the axially varying factor of the solution.

A. Problem formulation

In order to simplify calculations in the remainder, Galbrun's equation is first rewritten in its mixed pressure-displacement form:

$$\begin{cases} D\dfrac{d^2\mathbf{w}}{dt^2} + \nabla p + (\nabla\cdot\mathbf{w})\nabla P - {}^T\nabla\mathbf{w}\cdot\nabla P = 0 \\ p + DC^2\nabla\cdot\mathbf{w} = 0 \end{cases} \tag{2.1}$$

Upper and lower case letters respectively denote mean flow and acoustic variables. In the following, the adjective "acoustic" may be a misnomer because it will be used to qualify any disturbance, although a perturbation wave is likely to be of vortical type also. D, C, P and $\mathbf{V}$ are the density, sound celerity, pressure and velocity of the mean flow. p and $\mathbf{w}$ are the pressure and displacement Lagrangian perturbations (this kind of perturbation is associated to the same particle, unlike standard Eulerian perturbations). In the harmonic case, assuming an $e^{-i\omega t}$ dependence, the material derivative is given by $d/dt = -i\omega + \mathbf{V}\cdot\nabla$. An axisymmetric duct geometry is assumed. Cylindrical coordinates (r,θ,z) will be used, where z is the duct axis. Figure 1 represents a slowly varying annular duct in the (r,z) cutting plane.

Based on the continuity of normal displacement[8], the general boundary conditions at walls is given by:

$$p = -i\omega Z_i \mathbf{w}\cdot\mathbf{n} \qquad \text{at } r = R_i \quad i = 1,2 \tag{2.2}$$

$\mathbf{n}$ is the outward normal from the fluid point of view. R_1 and R_2 denote the inner and outer duct radii. Z_1 and Z_2 are the wall impedances at r=R_1 and R_2 respectively. R_i and Z_i may vary slowly along the duct axis.

The assumption of a slowly varying duct geometry suggests the use of a multiple-scales method, which first consists in defining the following slow spatial scale:

$$Z = \varepsilon z \quad , \quad \partial/\partial z = \varepsilon\, \partial/\partial Z \tag{2.3}$$

ε is a small parameter that can be quantified by the maximum axial slope of duct walls. Moreover, approximate solutions of the acoustic fields are sought of the following form:

$$\varphi(r,\theta,z,t) = \varphi(r,z) e^{i\int^z k_z(\alpha)d\alpha} e^{i(m\theta-\omega t)} \tag{2.4}$$

k_z represents the local axial wave number (unlike for a straight duct, k_z is slowly varying along the axis). m is the azimuthal mode number. Suppressing the exponential, derivation rules with respect to z becomes formally:

$$\frac{\partial \varphi}{\partial z} = ik_z\varphi + \varepsilon \frac{\partial \varphi}{\partial Z} \tag{2.5}$$

Concerning the mean flow, stationarity and θ-independence are supposed. Then, the application of a multiple-scales method to the basic equations of fluid mechanics shows that mean flow variables have the following expansions (see Refs. 6 and 13):

$$\begin{cases} D(r,Z;\varepsilon) = D_0(r,Z) + O(\varepsilon^2) \\ C(r,Z;\varepsilon) = C_0(r,Z) + O(\varepsilon^2) \\ P(r,Z;\varepsilon) = P_0(r,Z) + O(\varepsilon^2) \end{cases} , \quad \begin{cases} V_r(r,Z;\varepsilon) = \varepsilon V_{r_1}(r,Z) + O(\varepsilon^3) \\ V_\theta(r,Z;\varepsilon) = V_{\theta_0}(r,Z) + O(\varepsilon^2) \\ V_z(r,Z;\varepsilon) = V_{z_0}(r,Z) + O(\varepsilon^2) \end{cases} \tag{2.6}$$

In the remainder of this section, indices will denote the expansion order. Mean flow variables are supposed to have been calculated beforehand.

Then, using (2.5) and the mean flow mass conservation $\nabla \cdot D\mathbf{V} = 0$ to leading order (order ε^1), it can be shown that the material second derivatives can be written, after some calculations:

$$D_0 \frac{d^2\varphi}{dt^2} = -D_0\Omega^2\varphi - i\varepsilon \frac{1}{\varphi}\left\{ \frac{\partial\left(D_0 V_{z_0} \Omega \varphi^2\right)}{\partial Z} + \frac{1}{r}\frac{\partial\left(rD_0 V_{r_1} \Omega \varphi^2\right)}{\partial r} \right\} + O\left(\varepsilon^2\right) \qquad (2.7)$$

$$\text{with: } \Omega = \omega - k_z V_{z_0} - \frac{m}{r} V_{\theta_0}$$

Finally, reporting (2.5), (2.6) and (2.7) into (2.1) yields the following system, up to first order:

$$\begin{cases} -D_0\Omega^2 w_r + \dfrac{\partial p}{\partial r} + \dfrac{\partial P_0}{\partial r}\left(\dfrac{w_r}{r} + \dfrac{im}{r} w_\theta + ik_z w_z \right) = \\ \qquad i\varepsilon \dfrac{1}{w_r}\left\{ \dfrac{\partial\left(D_0 V_{z_0} \Omega {w_r}^2\right)}{\partial Z} + \dfrac{1}{r}\dfrac{\partial\left(rD_0 V_{r_1} \Omega {w_r}^2\right)}{\partial r} \right\} + \varepsilon\left\{ \dfrac{\partial P_0}{\partial Z}\dfrac{\partial w_z}{\partial r} - \dfrac{\partial P_0}{\partial r}\dfrac{\partial w_z}{\partial Z} \right\} \\ -D_0\Omega^2 w_\theta + \dfrac{im}{r} p - \dfrac{\partial P_0}{\partial r}\left(\dfrac{im}{r} w_r - \dfrac{w_\theta}{r} \right) = \\ \qquad i\varepsilon \dfrac{1}{w_\theta}\left\{ \dfrac{\partial\left(D_0 V_{z_0} \Omega {w_\theta}^2\right)}{\partial Z} + \dfrac{1}{r}\dfrac{\partial\left(rD_0 V_{r_1} \Omega {w_\theta}^2\right)}{\partial r} \right\} + \varepsilon \dfrac{\partial P_0}{\partial Z}\dfrac{im}{r} w_z \\ -D_0\Omega^2 w_z + ik_z p - \dfrac{\partial P_0}{\partial r} ik_z w_r = i\varepsilon \dfrac{1}{w_z}\left\{ \dfrac{\partial\left(D_0 V_{z_0} \Omega {w_z}^2\right)}{\partial Z} + \dfrac{1}{r}\dfrac{\partial\left(rD_0 V_{r_1} \Omega {w_z}^2\right)}{\partial r} \right\} \\ \qquad + \varepsilon\left\{ -\dfrac{\partial p}{\partial Z} - \dfrac{\partial P_0}{\partial Z}\left(\dfrac{1}{r}\dfrac{\partial}{\partial r}\left(rw_r\right) + \dfrac{im}{r} w_\theta \right) + \dfrac{\partial P_0}{\partial r}\dfrac{\partial w_r}{\partial Z} \right\} \\ p + D_0 C_0^2 \left(\dfrac{1}{r}\dfrac{\partial}{\partial r}\left(rw_r\right) + \dfrac{im}{r} w_\theta + ik_z w_z \right) = -\varepsilon D_0 C_0^2 \dfrac{\partial w_z}{\partial Z} \end{cases} \qquad (2.8)$$

Concerning the boundary condition (2.2), the outward normal is:

$$\mathbf{n}_i = \mp \frac{1}{\sqrt{1+\left(\frac{dR_i}{dz}\right)^2}} \left(\mathbf{e}_r - \frac{dR_i}{dz} \mathbf{e}_z \right) \qquad i = 1,2 \tag{2.9}$$

where the minus (resp. plus) sign is associated to i=1 (resp. i=2). Then, applying (2.3), the condition (2.2) becomes:

$$p = \pm i\omega Z_i \left(w_r - \varepsilon \frac{dR_i}{dZ} w_z \right) \qquad \text{at } r = R_i \qquad i = 1,2 \tag{2.10}$$

In order to obtain an approximate solution of **w** and p, acoustic variables are now expanded in powers of ε such that:

$$\begin{Bmatrix} w_r \\ w_\theta \\ w_z \\ p \end{Bmatrix} = \begin{Bmatrix} w_{r_0} \\ w_{\theta_0} \\ w_{z_0} \\ p_0 \end{Bmatrix} + \varepsilon \begin{Bmatrix} w_{r_1} \\ w_{\theta_1} \\ w_{z_1} \\ p_1 \end{Bmatrix} + O\left(\varepsilon^2\right) \tag{2.11}$$

B. Local solution at the order O(1)

Applying the expansion (2.11) to the system (2.8), we obtain to leading order (order ε^0):

$$\begin{cases} -D_0\Omega^2 w_{r_0} + \dfrac{\partial p_0}{\partial r} + \dfrac{\partial P_0}{\partial r}\left(\dfrac{w_{r_0}}{r} + \dfrac{im}{r} w_{\theta_0} + ik_z w_{z_0} \right) = 0 \\ -D_0\Omega^2 w_{\theta_0} + \dfrac{im}{r} p_0 - \dfrac{\partial P_0}{\partial r}\left(\dfrac{im}{r} w_{r_0} - \dfrac{w_{\theta_0}}{r} \right) = 0 \\ -D_0\Omega^2 w_{z_0} + ik_z p_0 - \dfrac{\partial P_0}{\partial r} ik_z w_{r_0} = 0 \\ p_0 + D_0 C_0^2 \left(\dfrac{1}{r}\dfrac{\partial}{\partial r}\left(r w_{r_0}\right) + \dfrac{im}{r} w_{\theta_0} + ik_z w_{z_0} \right) = 0 \end{cases} \tag{2.12}$$

The azimuthal and axial components of the displacement may be expressed in terms of the pressure and radial displacement, thanks to the second and third equations of the above system:

$$w_{\theta_0} = \frac{im}{r} \frac{p_0 - \dfrac{\partial P_0}{\partial r} w_{r_0}}{D_0\Omega^2 - \dfrac{1}{r}\dfrac{\partial P_0}{\partial r}} \quad , \quad w_{z_0} = ik_z \frac{p_0 - \dfrac{\partial P_0}{\partial r} w_{r_0}}{D_0\Omega^2} \tag{2.13}$$

Now, the system (2.12) can be simplified to a system of two differential equations by replacing the azimuthal and axial displacements (2.13) into the first and fourth equations of (2.12). This leads to:

$$\begin{cases} \alpha \dfrac{1}{r}\dfrac{\partial}{\partial r}\left(r w_{r_0}\right) + \beta \dfrac{\partial P_0}{\partial r} w_{r_0} + \left\{ \dfrac{\alpha}{D_0 C_0^2} - \beta \right\} p_0 = 0 \\ \alpha \dfrac{\partial p_0}{\partial r} - \beta \dfrac{\partial P_0}{\partial r} p_0 + \left\{ \beta \left(\dfrac{\partial P_0}{\partial r} \right)^2 - \alpha^2 \right\} w_{r_0} = 0 \end{cases} \tag{2.14}$$

$$\text{with:} \quad \alpha = D_0\Omega^2 - \frac{1}{r}\frac{\partial P_0}{\partial r} \quad , \quad \beta = \frac{m^2}{r^2} + k_z^2 - \frac{1}{r D_0\Omega^2}\frac{\partial P_0}{\partial r} k_z^2$$

Boundary condition (2.10) to leading order is simply given by:

$$p_0 = \pm i\omega Z_i w_{r_0} \quad \text{at} \quad r = R_i \qquad (i = 1, 2) \tag{2.15}$$

Equations (2.14) and (2.15) constitutes an eigenvalue problem (k_z is the eigenvalue) of two first order differential equations with two eigenfunctions, p_0 and w_{r_0}. However, this problem is unidimensional (r-dependent only) and is obviously not sufficient to give a complete solution of our problem. In fact, Eqs (2.14) and (2.15) must be solved for each cross-section of the duct (the duct axis being discretized) in order to obtain the radial profiles of the acoustic fields $\mathbf{w}_0(r)$ and $p_0(r)$. As explained in the following, the z-dependence of the acoustic variables will be obtained by means of a solvability condition derived from the first order problem.

It has to be outlined that system (2.14) can be further transformed into a single differential equation written in terms of p_0 only (See Appendix). Nevertheless, this does not really simplify the equations to solve because the single differential equation becomes of second order and the boundary condition, which would then have to be expressed in terms of pressure only, has a more complex form.

C. Solvability condition

Applying (2.11) to (2.8), the problem to first order ε^1 is given by:

$$L\psi_1 = f_0 \tag{2.16}$$

with the following notations:

$$L=\begin{bmatrix} -D_0\Omega^2+\dfrac{1}{r}\dfrac{\partial P_0}{\partial r} & i\dfrac{m}{r}\dfrac{\partial P_0}{\partial r} & ik_z\dfrac{\partial P_0}{\partial r} & \dfrac{\partial}{\partial r} \\ -i\dfrac{m}{r}\dfrac{\partial P_0}{\partial r} & -D_0\Omega^2+\dfrac{1}{r}\dfrac{\partial P_0}{\partial r} & 0 & i\dfrac{m}{r} \\ -ik_z\dfrac{\partial P_0}{\partial r} & 0 & -D_0\Omega^2 & ik_z \\ -\dfrac{1}{r}\dfrac{\partial\left(r(\cdot)\right)}{\partial r} & -i\dfrac{m}{r} & -ik_z & -\dfrac{1}{D_0C_0^2} \end{bmatrix}, \quad \psi_1=\begin{Bmatrix} w_{r_1} \\ w_{\theta_1} \\ w_{z_1} \\ p_1 \end{Bmatrix}$$

$$f_0=\begin{Bmatrix} i\dfrac{1}{w_{r_0}}\left\{\dfrac{\partial\left(D_0V_{z_0}\Omega w_{r_0}^2\right)}{\partial Z}+\dfrac{1}{r}\dfrac{\partial\left(rD_0V_{r_1}\Omega w_{r_0}^2\right)}{\partial r}\right\}+\dfrac{\partial P_0}{\partial Z}\dfrac{\partial w_{z_0}}{\partial r}-\dfrac{\partial P_0}{\partial r}\dfrac{\partial w_{z_0}}{\partial Z} \\ i\dfrac{1}{w_{\theta_0}}\left\{\dfrac{\partial\left(D_0V_{z_0}\Omega w_{\theta_0}^2\right)}{\partial Z}+\dfrac{1}{r}\dfrac{\partial\left(rD_0V_{r_1}\Omega w_{\theta_0}^2\right)}{\partial r}\right\}+\dfrac{\partial P_0}{\partial Z}\dfrac{im}{r}w_{z_0} \\ i\dfrac{1}{w_{z_0}}\left\{\dfrac{\partial\left(D_0V_{z_0}\Omega w_{z_0}^2\right)}{\partial Z}+\dfrac{1}{r}\dfrac{\partial\left(rD_0V_{r_1}\Omega w_{z_0}^2\right)}{\partial r}\right\}-\dfrac{\partial p_0}{\partial Z}-\dfrac{\partial P_0}{\partial Z}\left(\dfrac{1}{r}\dfrac{\partial}{\partial r}\left(rw_{r_0}\right)+\dfrac{im}{r}w_{\theta_0}\right)+\dfrac{\partial P_0}{\partial r}\dfrac{\partial w_{r_0}}{\partial Z} \\ \dfrac{\partial w_{z_0}}{\partial Z} \end{Bmatrix} \tag{2.17}$$

To first order, the boundary condition (2.10) is now:

$$p_1 \mp i\omega Z_i w_{r_1} = \mp i\omega Z_i \frac{dR_i}{dZ} w_{z_0} \qquad \text{at } r=R_i \qquad i=1,2 \tag{2.18}$$

L is not a self-adjoint operator. Thus, we must solve the adjoint problem, denoted by the exponent $\dagger$, and which satisfies the following identity:

$$\left\langle \psi_0^\dagger, L\psi_0 \right\rangle = \left\langle L^\dagger\psi_0^\dagger, \psi_0 \right\rangle \tag{2.19}$$

where the inner product is suitably defined by:

$$\left\langle A, B \right\rangle = \int_{R_1}^{R_2} \sum_{n=1}^{4} A_n^* B_n r dr \tag{2.20}$$

The exponent * denotes the complex conjugate. The following notations have been chosen for the eigenfunction and its adjoint:

$$\psi_0 = \left\langle w_{r_0}, w_{\theta_0}, w_{z_0}, p_0 \right\rangle \quad , \quad \psi_0^\dagger = \left\langle w_{r_0}^\dagger, w_{\theta_0}^\dagger, w_{z_0}^\dagger, p_0^\dagger \right\rangle \tag{2.21}$$

Then, after integrating by part terms in r-derivatives of the left-hand side of (2.19), and taking into account the fact that $L\psi_0=0$ – see Eq. (2.12) – and of Eq. (2.15), it can be shown that the adjoint problem is given explicitly by:

$$\begin{cases} L^{\dagger *}\psi_0^{\dagger *} = 0 \\ p_0^{\dagger *} = \pm i\omega Z_i w_{r_0}^{\dagger *} \qquad \text{at} \quad r = R_i \qquad (i = 1,2) \end{cases} \tag{2.22}$$

where the adjoint operator $L^\dagger$ is:

$$L^\dagger = \begin{bmatrix} -D_0\Omega^{*2} + \dfrac{1}{r}\dfrac{\partial P_0}{\partial r} & i\dfrac{m}{r}\dfrac{\partial P_0}{\partial r} & ik_z^*\dfrac{\partial P_0}{\partial r} & \dfrac{\partial}{\partial r} \\ -i\dfrac{m}{r}\dfrac{\partial P_0}{\partial r} & -D_0\Omega^{*2} + \dfrac{1}{r}\dfrac{\partial P_0}{\partial r} & 0 & i\dfrac{m}{r} \\ -ik_z^*\dfrac{\partial P_0}{\partial r} & 0 & -D_0\Omega^{*2} & ik_z^* \\ -\dfrac{1}{r}\dfrac{\partial \left(r(\cdot)\right)}{\partial r} & -i\dfrac{m}{r} & -ik_z^* & -\dfrac{1}{D_0C_0^2} \end{bmatrix} \tag{2.23}$$

Solution of the adjoint problem (2.22) is then simply given by:

$$w_{r_0}^{\dagger *} = w_{r_0} \quad , \quad w_{\theta_0}^{\dagger *} = -w_{\theta_0} \quad , \quad w_{z_0}^{\dagger *} = -w_{z_0} \quad , \quad p_0^{\dagger *} = p_0 \tag{2.24}$$

This can be easily verified by reporting (2.24) into (2.22) and by verifying that the system thus obtained is strictly equivalent to (2.12) and (2.15).

Then, the solvability condition is obtained by integrating by part the inner product between $\psi_0^\dagger$ and $L\psi_1$, which gives:

$$\left\langle \psi_0^\dagger, L\psi_1 \right\rangle = \underbrace{\left\langle L^\dagger \psi_0^\dagger, \psi_1 \right\rangle}_{=0} + \left[-rp_0^{\dagger *} w_{r_1} + rw_{r_0}^{\dagger *} p_1 \right]_{R_1}^{R_2} \tag{2.25}$$

Making use of (2.24) and of the boundary condition to leading order (2.15), as well as to first order (2.18), the equality (2.25) becomes:

$$\left\langle \psi_0^\dagger, L\psi_1 \right\rangle = i\omega Z_2 R_2 \frac{dR_2}{dZ} w_{r_0} w_{z_0} \Big|_{r=R_2} + i\omega Z_1 R_1 \frac{dR_1}{dZ} w_{r_0} w_{z_0} \Big|_{r=R_1} \tag{2.26}$$

The left-hand side of the above equation can also be explicitly calculated, knowing that $L\psi_1 = f_0$ and relations (2.24). After some rearrangements, this yields:

$$\begin{aligned} \left\langle \psi_0^\dagger, L\psi_1 \right\rangle = \int_{R_1}^{R_2} \Bigg\{ & i\left[\frac{\partial}{\partial Z}\left\{ D_0 V_{z_0} \Omega \left(w_{r_0}^2 - w_{\theta_0}^2 - w_{z_0}^2 \right) \right\} + \frac{1}{r}\frac{\partial}{\partial r}\left\{ rD_0 V_{r_1} \Omega \left(w_{r_0}^2 - w_{\theta_0}^2 - w_{z_0}^2 \right) \right\} \right] \\ & + \frac{\partial}{\partial Z}\left(p_0 w_{z_0} \right) + \frac{1}{r}\frac{\partial}{\partial r}\left(\frac{\partial P_0}{\partial Z} r w_{r_0} w_{z_0} \right) - \frac{\partial}{\partial Z}\left(\frac{\partial P_0}{\partial r} w_{r_0} w_{z_0} \right) \Bigg\} rdr \end{aligned} \tag{2.27}$$

Terms in $\partial/\partial r$ are integrated in a straightforward way. For terms in $\partial/\partial Z$, Leibniz formula is used:

$$\int_{R_1(Z)}^{R_2(Z)} \frac{\partial}{\partial Z} f(r,Z) dr = \frac{d}{dZ} \int_{R_1(Z)}^{R_2(Z)} f(r,Z) dr - \left[\frac{dR(Z)}{dZ} f(Z,R) \right]_{R_1(Z)}^{R_2(Z)} \tag{2.28}$$

Using (2.28) into (2.27), and using (2.15), again leads to:

$$\begin{aligned}\left\langle \psi_0^\dagger, L\psi_1 \right\rangle = &\frac{d}{dZ}\int_{R_1}^{R_2}\left\{ iD_0 V_{z_0}\Omega\left(w_{r_0}^2 - w_{\theta_0}^2 - w_{z_0}^2\right) + p_0 w_{z_0} - \frac{\partial P_0}{\partial r} w_{r_0} w_{z_0} \right\} r dr \\ &+ \left[iD_0 r\Omega\left(V_{r_1} - \frac{dR}{dZ} V_{z_0} \right)\left(w_{r_0}^2 - w_{\theta_0}^2 - w_{z_0}^2\right) \right]_{R_1}^{R_2} \\ &+ i\omega Z_2 R_2 \frac{dR_2}{dZ} w_{r_0} w_{z_0}\bigg|_{r=R_2} + i\omega Z_1 R_1 \frac{dR_1}{dZ} w_{r_0} w_{z_0}\bigg|_{r=R_1} \\ &+ \left(R_2 w_{r_0} w_{z_0}\left\{ \frac{\partial P_0}{\partial Z} - \frac{dR_2}{dZ}\frac{\partial P_0}{\partial r} \right\} \right)\bigg|_{r=R_2} - \left(R_1 w_{r_0} w_{z_0}\left\{ \frac{\partial P_0}{\partial Z} - \frac{dR_1}{dZ}\frac{\partial P_0}{\partial r} \right\} \right)\bigg|_{r=R_1}\end{aligned} \tag{2.29}$$

Now, the boundary condition for the mean flow is $\mathbf{V}\cdot\mathbf{n} = 0$ at $r=R_i$, which gives to leading order (order ε^1):

$$V_{r_1} - \frac{dR_i}{dZ} V_{z_0} = 0 \quad \text{at} \quad r = R_i \qquad (i = 1,2) \tag{2.30}$$

The above condition makes the second line of Eq. (2.29) vanish. Then, it has to be noted that the radial mean flow velocity completely disappears from expression (2.29), which renders its calculation unnecessary.

Finally, combining equalities (2.26) and (2.29) leads to the following rather simple solvability condition:

$$\begin{aligned}&\frac{d}{dZ}\int_{R_1}^{R_2}\left\{ iD_0 V_{z_0}\Omega\left(w_{r_0}^2 - w_{\theta_0}^2 - w_{z_0}^2\right) + p_0 w_{z_0} - \frac{\partial P_0}{\partial r} w_{r_0} w_{z_0} \right\} r dr \\ &+ \left(R_2 w_{r_0} w_{z_0}\left\{ \frac{\partial P_0}{\partial Z} - \frac{dR_2}{dZ}\frac{\partial P_0}{\partial r} \right\} \right)\bigg|_{r=R_2} - \left(R_1 w_{r_0} w_{z_0}\left\{ \frac{\partial P_0}{\partial Z} - \frac{dR_1}{dZ}\frac{\partial P_0}{\partial r} \right\} \right)\bigg|_{r=R_1} = 0\end{aligned} \tag{2.31}$$

D. Multiple-scales solution

Mode-like displacement and pressure variables that we are looking for are rewritten as follows:

$$\begin{cases} p_0(r,Z) = A_0(Z)\, p_0(r) \\ w_{r_0}(r,Z) = A_0(Z)\, w_{r_0}(r) \\ w_{\theta_0}(r,Z) = A_0(Z)\, w_{\theta_0}(r) \\ w_{z_0}(r,Z) = A_0(Z)\, w_{z_0}(r) \end{cases} \tag{2.32}$$

where $p_0(r)$ and $\mathbf{w}_0(r)$ correspond to the local eigenfunctions obtained from Eq. (2.14) and (2.15). $A_0(Z)$ is an axially amplitude function to solve. Replacing acoustic variables (2.32) into the solvability condition (2.31) and making use of expressions (2.13) gives the following differential equation for the unknown $A_0(Z)^2$:

$$\frac{d}{dZ}\left[\gamma(Z) A_0(Z)^2\right] = \lambda(Z) A_0(Z)^2 \tag{2.33}$$

where γ and λ only depend upon Z, and are given by:

$$\begin{aligned} \gamma(Z) &= \int_{R_1}^{R_2} iD_0 V_{z_0} \Omega \left[w_{r_0}^2 + \frac{1}{D_0^2 \Omega^4} \left(p_0 - \frac{\partial P_0}{\partial r} w_{r_0} \right)^2 \left\{ \frac{m^2}{r^2} \left(1 - \frac{1}{r D_0 \Omega^2} \frac{\partial P_0}{\partial r} \right)^{-2} + k_z^2 + k_z \frac{\Omega}{V_{z_0}} \right\} \right] r dr \\ \lambda(Z) &= \sum_{i=1}^{2} \left(\frac{R_i k_z}{\omega Z_i D_0 \Omega^2} p_0 \left(p_0 - \frac{\partial P_0}{\partial r} w_{r_0} \right) \left\{ \frac{\partial P_0}{\partial Z} - \frac{dR_i}{dZ} \frac{\partial P_0}{\partial r} \right\} \right)_{|r=R_i} \end{aligned} \tag{2.34}$$

The general solution of Eq. (2.33) is:

$$A_0(Z)^2 = N_0^2 \exp \int^Z \frac{\lambda(x) - \gamma'(x)}{\gamma(x)} dx \tag{2.35}$$

where N_0^2 denotes a normalization factor (constant of integration).

From a computational point of view, the solving method is as follows. Equations are adimensionalized. First, the local eigenvalue problem given by Eq. (2.14) and (2.15) is solved for each duct cross-section by an iterative Runge-Kutta algorithm. Then, knowing $p_0(r)$, $\mathbf{w}_0(r)$ and $k_z(Z)$, a numerical 1D integration with respect to r is used to compute $\gamma(Z)$ from Eq. (2.34). Finally, given $\gamma(Z)$ and $\lambda(Z)$, another 1D integration (with respect to Z this time) is computed in order to obtain $A_0(Z)$ from Eq. (2.35). The complete solution is provided by (2.32) multiplied by the exponential factors of Eq. (2.4).

As stated earlier, this section has assumed that the mean flow was initially computed. Except some physical and realistic conditions the mean flow has to satisfy – Eq. (2.30) and mass conservation used for (2.7) – the proposed multiple-scales solution is valid for any arbitrary mean flow. In particular, it remains also valid for non-homentropic flows, unlike Cooper and Peake's solution[6]. Moreover, the local eigenvalue problem consists in solving two differential equations, instead of four for Cooper and Peake's solution, and the solvability condition seems to be simpler to compute.

However, for conciseness and clarity, no turning points analysis has been included here, the main point of the paper being to compare the MS solution with a FEM model. Turning points occurs when a mode changes from cut-on to cut-off inside the duct. For this peculiar case, the proposed MS approximation breaks down and the method needs some adaptation (see for instance Ref. 6).

III. FEM model

In this section, the FEM proposed to study sound propagation in arbitrary flows is briefly recalled. The numerical method has already been developed in authors' recent papers[18,19], to which the reader is referred for more details. Unlike the multiple-scales model, the developed FEM is valid for any varying duct geometry (not necessarily slowly varying).

A. Problem formulation

A typical duct is depicted on Fig. 1. The geometry is axisymmetric and sketched on the (r,z) cutting plane. Ω_a denotes the fluid domain. Boundary notations correspond to different types of boundary conditions, as defined in the following.

Differential equations governing acoustics in Ω_a has already been given by Eqs. (2.1). An $e^{-i\omega t}$ harmonic regime is assumed. The mean flow is supposed to be stationary. Two kinds of boundary conditions may be defined: a prescribed displacement condition and an absorbing wall condition. The former may be imposed at both the inlet and the outlet. These conditions are respectively given by:

$$\mathbf{w} = \overline{\mathbf{w}} \quad \text{on } \Gamma_w \tag{3.1}$$

$$\mathbf{w}\cdot\mathbf{n} = -\frac{1}{i\omega Z}\,p \quad \text{on } \Gamma_i \tag{3.2}$$

Note that the above impedance condition is based on the normal Lagrangian displacement continuity[8]. For a perfectly rigid wall, i.e. $Z\to\infty$, Eq. (3.2) reduces to $\mathbf{w}\cdot\mathbf{n} = 0$.

It must be emphasized that a prescribed outlet displacement implies that we already know the solution at the outlet, which is not very satisfying from a physical point of view. Indeed, as explained in Sec. IV, a modal decomposition will be preferred at the duct outlet in order to simulate a multi-modal non-reflecting boundary condition.

B. Variational formulation

Though a purely displacement formulation can be derived from (2.1) (see for instance Refs. 10 or 23), a mixed pressure-displacement variational formulation is preferred in order to avoid spurious numerical solutions, known in literature as a "locking" phenomenon[24].

Equations (2.1) are respectively multiplied by two trial fields, $\mathbf{w}^*$ and p^*, and integrated over Ω_a. Integrating by parts and applying boundary conditions (3.1) and (3.2) yields the following variational problem, which consists in solving the acoustic variables $\{\mathbf{w}, p\}$ verifying $\left\{\mathbf{w}|_{\Gamma_w} = \overline{\mathbf{w}}\right\}$ and:

$$
\begin{aligned}
&-\int_{\Omega_a}\frac{1}{DC^2}p^*pdV+\int_{\Omega_a}\nabla p^*\cdot\mathbf{w}dV+\int_{\Omega_a}\mathbf{w}^*\cdot\nabla pdV-\omega^2\int_{\Omega_a}D\mathbf{w}^*\cdot\mathbf{w}dV\\
&-i\omega\int_{\Omega_a}D\mathbf{w}^*\cdot\left(\mathbf{V}\cdot\nabla\mathbf{w}\right)dV+i\omega\int_{\Omega_a}D\left(\mathbf{V}\cdot\nabla\mathbf{w}^*\right)\cdot\mathbf{w}dV-\int_{\Omega_a}D\left(\mathbf{V}\cdot\nabla\mathbf{w}^*\right)\cdot\left(\mathbf{V}\cdot\nabla\mathbf{w}\right)dV\\
&+\int_{\Omega_a}\left(\mathbf{w}^*\cdot\nabla P\right)\left(\nabla\cdot\mathbf{w}\right)dV-\int_{\Omega_a}\mathbf{w}^*\cdot\left({}^T\nabla\mathbf{w}\cdot\nabla P\right)dV\\
&-\int_{\Gamma_w}p^*\left(\mathbf{w}\cdot\mathbf{n}\right)dS+\frac{1}{i\omega}\int_{\Gamma_i}\frac{1}{Z}p^*pdS=0\qquad\qquad\forall\mathbf{w}^*,p^*\Big/\left\{\mathbf{w}^*\big|_{\Gamma_w}=0\right\}
\end{aligned}
\tag{3.3}
$$

The first line represents the no-flow acoustic operators, the second gives the additional operators when flow is present. The last line is a boundary integral, on which boundary conditions are imposed. Note that impermeable walls have been assumed so that $\mathbf{V}\cdot\mathbf{n}=0$ on Γ_i.

The third line corresponds to operators that have to be included when the mean pressure is not spatially constant. For simplicity, those operators were not considered in previous papers[10,18] because they do a priori not represent any difficulty from a numerical point of view. In this paper, results tend to prove that this statement is actually true. Unlike Refs. 18 and 19, it is important to note that no assumption is made here for the mean flow (except its stationarity), so that formulation (3.3) is quite general and, in particular, takes into account compressibility effects of the mean flow. Thus, mean density, sound celerity, pressure and velocity can arbitrarily vary inside the duct.

C. Finite element discretization

The geometry is assumed to be axisymmetric. Without loss of generality, fluctuating variables can be rewritten in the following form:

$$(\mathbf{w}, p)(r,\theta,z,t) = (\mathbf{w}, p)(r,z)e^{i(m\theta-\omega t)} \tag{3.4}$$

Trial functions are given by:

$$(\mathbf{w}^*, p^*)(r,\theta,z,t) = (\mathbf{w}^*, p^*)(r,z)e^{-i(m\theta-\omega t)} \tag{3.5}$$

In order to avoid locking and spurious solutions, interpolations for displacement and pressure variables must also be adequately chosen. Though not necessary, a criterion that ensures convergence and stability of the finite element is given by the inf-sup condition, well-known for incompressible media (see for instance Ref. 24). This kind of finite element has already been successfully applied to the variational formulation (3.3) in the constant P case, when testing the effect of shear flows[18,19].

The element chosen in this paper, referred to as the "P_1^+-P_1", "4/3c" or "MINI" element in the literature, is a three-node triangle with an internal degree of freedom for each component of the displacement. Its interpolating functions are, on the reference element:

$$\begin{cases} \mathbf{w}(u,v) = (1-u-v)\mathbf{w}_1 + u\mathbf{w}_2 + v\mathbf{w}_3 + (1-u-v)uv\mathbf{a} \\ p(u,v) = (1-u-v)p_1 + up_2 + vp_3 \end{cases} \tag{3.6}$$

where the subscripts i (i=1,2,3) denote node number. $\mathbf{a}$ is a generalized variable corresponding to an internal degree of freedom, which can be condensed out before the elements are assembled. As a side remark, the overall method presented in this paper is

easily applicable to the 3D case because elements satisfying the inf-sup condition also exists in three dimensions[24].

After assembling and applying boundary conditions, the global discretized variational formulation yields an algebraic system of the **Ku=f** form, where **u** contains all the acoustic nodal unknowns (displacement and pressure). The matrix **K** is ω-dependent, unsymmetrical, complex and band. A sparse storage is chosen. For a fixed ω, the unknown nodal vector **u** is finally obtained by using a LU decomposition.

IV. RESULTS

In this section, both MS and FEM models are compared. Acoustic computations are made for perfectly rigid and lined ducts, in the presence of compressible flows with swirl.

A. Preliminary remarks

Boundary conditions used for FEM calculations are shown on Fig. 1. At the duct inlet (from an acoustical point of view), Lagrangian displacement calculated from the MS solution is prescribed. In the following, the acoustic inlet will always be at the top section z=2 m. At the outlet (z=0m), a multi-modal decomposition technique is used.

This technique consists in recasting the nodal acoustic variables located at the duct outlet via an eigenmode expansion (see for example Refs. 25, 26). This technique was also satisfyingly used in Ref. 18 to simulate a multi-modal non-reflecting boundary condition, with non-swirling flows. Here, the method is extended to swirling flows. In this paper, five radial modes have been used for the decomposition, which is far enough given that higher order modes are strongly cut-off for the considered test cases (it must be noted that no azimuthal decomposition is needed because m is a fixed parameter in the axisymmetric FEM code).

The reason why a multi-modal non-reflecting condition is used at the outlet comes from reflection and scattering into other modes that may occur when the launched mode propagates along the duct. The FEM model naturally includes any reflection and scattering. This is not the case for the MS model, which implicitly assumes a one-way propagating mode, neglecting reflection and scattering[18,25]. Thus, Forcing the Lagrangian displacement (calculated from the MS model) at the outlet too would not be very satisfying from a physical point of view, nor would be a mono-modal non-reflecting condition.

However, applying a modal decomposition technique raises the problem of mode orthogonality and completeness. For non-swirling flows, modes are orthogonal if the axial mean flow is uniform at the duct section being considered (as well as mean density, celerity and pressure). For swirling flows, as shown in Appendix, the flow must also be

in rigid-body rotation. For our purpose, this means that the mean flow at the outlet must be uniform in its axial direction, in rigid-body rotation and that density, celerity and pressure remains also constant.

Consequently, mean flows considered in this paper are restricted to this particular form at the outlet. They are calculated from the aerodynamic MS model of Cooper and Peake[6]. This model provides aerodynamic solutions for slowly varying ducts in the fully compressible case with the assumption of homentropy (yet, we recall that the acoustic MS model proposed in this paper remains valid even for non-homentropic mean flows). Solutions have the particularity to be nearly-uniform at the computing starting point, here at the outlet z=0m, and hence to satisfy all the requiring conditions needed to use the above-mentioned non-reflecting condition. To be quantitatively more precise, for results presented in the following, mean flow density, celerity and pressure vary up to 5% from their respective mean at the outlet. Variations of the axial velocity and rotation are almost of 0%. Then, the MS model yields acoustic modes which axial wavenumbers have a 4% maximum difference from the uniform flow case, with quasi-identical pressure profiles.

Inputs of Cooper and Peake's aerodynamic MS model are the outlet axial Mach number $M_0 = V_z / C^*$ and the outlet azimuthal Mach number defined as $\Omega_0 = V_\theta L^* / rC^*$, where C^* and L^* denote respectively the characteristic sound speed and length. In this

paper, C^*=340m.s^{-1} and L^*=1m. In all test cases given below, the computed density D remains about 1.2kg.m^{-3} throughout the fluid, C and P are about 340m.s^{-1} and 10^5 Pa.

The geometry considered is the same as in Ref. 6. This is a slowly varying duct, contracting or expanding, defined by its inner and outer radii as:

$$\begin{cases} R_1(z) = 0.5482 \pm 0.05\tanh(2z-2) \\ R_2(z) = 1.1518 \mp 0.05\tanh(2z-2) \end{cases} \tag{4.1}$$

In the following, iso-pressure contours are given in Pa in order not to minimize errors. Propagation and axial flow directions are also sketched in order to explicitly show if wave propagation is upstream or downstream. Test cases sweep a non-dimensional frequency range up to about kL^*=30 and the duct geometry is generally meshed with a $\lambda/10$ finite element length. Figure 2 exhibits two examples of $\lambda/10$ meshes used in this paper.

B. Comparison for perfectly rigid ducts

The first example is that of a (−5,1) mode propagating in a perfectly rigid and expanding duct with M_0=−0.21 and Ω_0=+0.30 at the outlet (z=0). A negative product $m\Omega_0$ means that the mode is counter-rotating. Figure 3 depicts all mean flow variables but radial velocity, which is negligible and not needed for acoustic MS solutions. At

z=0m, it can be observed that the axial velocity is uniform and that the azimuthal velocity profile varies linearly, indicating a rigid-body rotation. Besides, density, celerity and pressure vary slowly. Thus, at z=0, a modal decomposition can be accurately made. At the inlet z=2m (from the acoustical point of view), the mean flow is not uniform any more, cross-sectional means of M_0 and Ω_0 are −0.30 and +0.30 respectively.

Figure 4 shows the acoustic results for both models and for f=350, 500 and 650Hz. A good agreement is found for every frequency. In particular, the (−5,1) mode is strongly attenuated at f=350Hz, indicating a cut-off. Cut-off frequencies can be approximated by the analytical expression (A.8) valid in the uniform case (if not uniform, the flow has then to be averaged at each section). This expression gives a local cut-off frequency of 361Hz and 391Hz at z=0 and 2m respectively, which confirms that the mode is evanescent throughout the duct (no turning point occurs).

Small discrepancies can be observed on Fig.4e near the modal pressure node (at $r \simeq 1.0$m). As shown on Fig.5, they almost disappear when the mesh is refined ($\lambda/10$ and $\lambda/20$ meshes have been used for Fig.4e and 5 respectively). In the remaining of this paper, analyses of convergence of the FEM implementation will not be pursued and are left for further studies. However, mesh refinements have been done for every test case of the present paper (though not shown for conciseness) in order to determine if the differences observed between solutions are physical or numerical. FEM results presented in this paper are given with a sufficiently small meshing (generally a $\lambda/10$ mesh), which

prevents discrepancies due to a convergence lack and truly enables a physical interpretation.

The second test case concerns a (+20,0) mode propagating in a contracting duct at f=1250, 1500 and 1750Hz (see Fig. 6). At z=0, the flow is nearly uniform, with M_0=+0.30 and Ω_0=+0.30 (at z=2m, their means are respectively +0.21 and +0.30). For conciseness, mean flow variables are not depicted any more in the following.

Both models converge in a satisfying way. A very slight difference may be seen at 1750Hz, which can be explained by some little reflections occurring inside the duct (not taken into account by the MS model). As previously, the mode being considered is cut-off for the lowest frequency f=1250Hz. The analytical cut-off frequency goes from 1304Hz at z=2m to 1367Hz at z=0m, which confirms the evanescence observed.

Figure 7 shows the axial time-averaged intensity for the three frequencies. The time-averaged intensity is post-processed from the FEM solution, and explicitly given by:

$$\bar{\mathbf{i}} = -\frac{\omega}{2}\mathrm{Im}\left\{\left(p-\mathbf{w}\cdot\nabla P\right)\mathbf{w}^* + D\left(\frac{d\mathbf{w}}{dt}\cdot\mathbf{w}^*\right)\mathbf{V}\right\} \tag{4.2}$$

In the above expression, $\mathbf{w}^*$ denotes the complex conjugate of $\mathbf{w}$ and must not be confused with the trial field of Eq. (3.3). Equation (4.2) derives from the intensity expression obtained from Galbrun's equation in Refs. 8 and 10. This expression is exact and quite general (but not unique).

The cut-off occurring at 1250Hz is well characterized by a negligible axial intensity compared to the two other frequencies. Note that this intensity is not equal to zero (but strongly decreases from the inlet) because, when flow is present, cut-off modes have a small propagative part (the axial wavenumber is not purely imaginary). Besides, as expected, axial intensity is slightly increased from 1500 to 1750Hz, because of the axial wavenumber increase with frequency.

It must be noted that, without swirl, the mode would be completely cut-on, even at 1250Hz (analytical cut-off frequency would be of about 1000Hz): what is seen at f=1250Hz is one of the swirl effects, which increases cut-off frequencies for co-rotating modes (i.e. with positive product $m\Omega_0$). This effect is thus correctly included in both MS and FEM models.

C. Comparison for lined ducts

In this subsection, lined ducts are considered. In the presence of treatment at walls, modes are not orthogonal in the usual sense, which may affect the efficiency of the non-reflecting boundary condition. The duct must then be perfectly rigid at the outlet z=0. However, in fact, the transition from impedance to rigid wall can be initiated at an arbitrarily small distance from the outlet, as stated in Ref. 25.

The third example gives a comparison for the (±3,0) modes propagating at f=200 and 300Hz, inside a contracting duct, with M_0=+0.52 and Ω_0=+0.20 at z=0m (at z=2m, averaged M_0 and Ω_0 are respectively +0.35 and +0.20). Walls are lined with impedances Z_1=Z_2=408−408i. As shown on Fig. 8, the agreement between both models is very good for every cases. In particular, axial attenuation satisfyingly converges (at 300Hz and for m=−3, the FEM model gives a very little smaller attenuation, probably due to some reflection inside the duct). This attenuation, denoted by μ in dB, can be explicitly computed with the following definition:

$$\mu = 10\log_{10}\left(\int_{R_1(0)}^{R_1(0)} \left|p(r,z=0)\right|^2 r dr \Big/ \int_{R_1(L)}^{R_1(L)} \left|p(r,z=L)\right|^2 r dr \right) \tag{4.3}$$

At 200Hz, the attenuation is about 40dB and 60dB for m=−3 and m+3 respectively. At 300Hz, it decreases to about 10 and 20dB. Those results confirm the general trend found by Cooper and Peake[6], indicating that co-rotating modes are always more damped than counter-rotating ones. This difference in damping may be important, as shown by the presented results. It becomes lower as frequency increases, going further and further from cut-off (cut-off frequencies for counter- and co-rotating modes are about 130 and 195Hz respectively).

Figure 9 exhibits the last test case: a (±10,1) mode propagating in a lined expanding duct at 850Hz. Flow parameters at z=0m are given by M_0=−0.35 and Ω_0=+0.2 (this yields averages of −0.52 and +0.2 at z=2m). Wall impedances are Z_1=Z_2=1020−1020i. In

order to explicitly show the effect of swirl, Fig. 9 gives a comparison between the three following modes: m=−10 (with swirl), m=10 without swirl, m=+10 (with swirl). Note that without swirl, the sign of m has no consequence upon the solution, and that the MS solution corresponds to Rienstra's solution[13] (mean flow variables do not depend upon r and are uniform upon each section).

The convergence between both models is rather good but some wiggles can be observed for FEM solutions, which are probably due to reflection and/or scattering into other modes. As explained earlier, it has been verified that the differences between MS and FEM solutions are not mesh related (refinements may yield some smoother profiles but they do not modify the overall results presented in this paper). For m=+10, almost no wiggles appear because this mode is near from its cut-off frequency (about 800Hz): the axial wavenumber k_z is then lower, which makes the effect of geometry axial variations less important upon acoustic wave propagation (reflections are negligible).

This example shows the effect of the presence of swirl compared to the no swirl case. Attenuation equals about 6, 7 and 15dB for m=−10, m=10 without swirl, and m=+10 respectively. Here again, the conclusion agrees with Cooper and Peake's results.

Figure 10 depicts the axial intensity post-processed from FEM solutions for the three modes. It can be observed that intensity is gradually decreased from m=−10 to m=+10. For m=+10, the axial intensity is very low because this mode is near from its

cut-off frequency (about 800Hz), which is not the case of modes m=−10 and m=10 without swirl (their respective cut-off occurs at about 570 and 690Hz). Moreover, an enlargement of intensity vector is also given, which shows that it is not parallel to the wall, meaning that some energy is absorbed. Note that the vector penetrates more into the walls for m=−10. Those energy considerations are coherent with the fact that attenuation is higher (resp. lower) for co-rotating (resp. counter-rotating) modes than in the no-swirl case.

V. CONCLUSION

In this paper, a MS method and a FEM have been proposed to study sound propagation in ducts with compressible and swirling flows. Both methods are based on Galbrun's equation, which provides some interesting aspects. Boundary conditions at lined walls have a simplified form, and exact expressions of intensity and energy are available. For the MS model, equations are easier to solve than those based on the standard linearized Euler equations. For the FEM model, a mixed pressure-displacement based formulation allows the direct application of the inf-sup condition, well-known for incompressible media.

The MS method applies for slowly varying duct, whereas the FEM model is quite general. In order to validate both models, a comparison between MS and FEM solutions has been realized for a slowly varying duct, expanding or contracting. A good agreement

has been found. Results presented in this paper show that both models are able to take into account the effects of swirl upon acoustic propagation, and that neglecting swirl in acoustics with flows may lead to significant errors. In particular, co-rotating (resp. counter-rotating) modes are likely to be cut-off (resp. cut-on) or, if the duct is lined, more (resp. less) damped compared to the no-swirl case. The importance that those effects may have shows the limitations inherent to a full-potential formulation, which assumes that both acoustic and aerodynamic velocities are irrotational. This justifies the use of more general equations, such as the linearized Euler equations or Galbrun's equation.

However, concerning FEM computations, the non-reflecting boundary condition used in this paper assumes a uniform and rigid-body rotation flow at the outlet (or nearly). Because its efficiency may be affected by stronger flow non-uniformities, the proposed non-reflecting boundary condition would a priori need some adaptation in order to be applied to any kind of flows.

APPENDIX: LOCAL EIGENPROBLEM

System (2.14) can be reduced to a single differential equation written in terms of p_0. From the second equation of (2.14), the radial displacement is:

$$w_{r_0} = \frac{\alpha \dfrac{\partial p_0}{\partial r} - \beta \dfrac{\partial P_0}{\partial r} p_0}{\alpha^2 - \beta \left(\dfrac{\partial P_0}{\partial r} \right)^2} \tag{A.1}$$

After some tedious calculations, replacing the radial displacement into the first equation of (2.14) leads to the following single differential equation for p_0:

$$\frac{\partial^2 p_0}{\partial r^2} + \left\{ \frac{1}{r} + \frac{-\alpha\alpha' + \left(\beta' + 2\beta P_0' - \alpha'\beta/\alpha\right) P_0'^2}{\alpha^2 - \beta P_0'^2} \right\} \frac{\partial p_0}{\partial r} + \left\{ \left(\frac{\alpha}{D_0 C_0^2} - \beta \right) \left(1 - \frac{\beta}{\alpha^2} P_0'^2 \right) \right.$$
$$\left. + \frac{\left(2\alpha'\beta - \alpha\beta'\right) P_0' - \alpha\beta \left(r P_0'\right)' / r - \left(\alpha^2 \beta - \beta^2 P_0'^2 + \alpha\beta r \left(P_0'/r\right)' \right) \beta P_0'^2 / \alpha^2}{\alpha^2 - \beta P_0'^2} \right\} p_0 = 0 \tag{A.2}$$

where primes refer to first and second partial derivatives (with respect to r) of the equation coefficients. Boundary condition (2.15) has also to be expressed in terms of p_0:

$$\frac{\partial p_0}{\partial r} = \mp \frac{i}{\omega Z_i \alpha} \left\{ \alpha^2 - \beta P_0'^2 \pm i\omega Z_i \beta P_0' \right\} p_0 \qquad \text{at} \quad r = R_i \qquad (i = 1,2) \tag{A.3}$$

In the specific case of a uniform flow defined by the fact that D_0, C_0, P_0, V_{z_0} and V_{θ_0}/r do not depend upon r (i.e. uniform axial velocity and rigid-body rotation), Eq. (A.2) reduces to:

$$\frac{\partial^2 p_0}{\partial r^2} + \frac{1}{r} \frac{\partial p_0}{\partial r} + \left\{ \frac{\Omega^2}{C_0^2} - \frac{m^2}{r^2} - k_z^2 \right\} p_0 = 0 \tag{A.4}$$

where Ω is now constant. Solutions of Eq. (A.4) are thus a combination of Bessel's functions:

$$p_{0_{mn}}(r) = A J_m\left(k_{r_{mn}} r\right) + B Y_m\left(k_{r_{mn}} r\right) \tag{A.5}$$

where the radial wave number is given by the dispersion equation:

$$k_{r_{mn}}^2 = \Omega^2 / C_0^2 - k_{z_{mn}}^2 \tag{A.6}$$

As for the no-flow case, the (m,n) modes are orthogonal when walls are perfectly rigid.

Furthermore, it can be shown from (A.6) that:

$$k_{z_{mn}}^{\pm} = \frac{-M_0 (k - mk_0) \pm \sqrt{(k - mk_0)^2 - (1 - M_0^2) k_{r_{mn}}^2}}{1 - M_0^2} \tag{A.7}$$

where $k=\omega/C_0$, $M_0=V_{z_0}/C_0$ and $k_0=V_{\theta_0}/r\,C_0$. This relation is the same that in Kerrebrock's analysis[1]. Cut-off frequencies of the (m,n) mode corresponds to the value of k for which term inside the square root vanishes (when perfectly rigid walls are considered). After some calculations, this leads to:

$$f_{c_{mn}} = \sqrt{1 - M_0^2}\, f_{0_{mn}} + \frac{m\omega_0}{2\pi} \tag{A.8}$$

where $\omega_0=V_{\theta_0}/r$. $f_{0_{mn}} = c_0 k_{r_{mn}}/2\pi$ is the no-flow cut-off frequency. This relation shows that cut-off frequencies are modulated by a $\sqrt{1-M_0^2}$ factor (for any direction of the axial flow) and incremented by $m\omega_0/2\pi$ (cut-off frequencies of counter-rotating modes are decreased, and vice-versa for co-rotating modes). This basic result is experienced in Sec. IV.

Assumptions used to obtain Eq. (A.4) may not be realistic from the mean flow point of view, because the mean pressure gradient is directly related to the presence of swirl[27] (if swirl is present, then the mean pressure can not be constant). Nevertheless, for acoustic computations, small mean pressure gradient may be neglected. Then, orthogonal properties of solution (A.5) and Eq. (A.8) may be very useful for acoustic computations and physical understanding, as proved in Sec. IV.

[1] J. L. Kerrebrock, "Small disturbances in turbomachine annuli with swirl," American Institute of Aeronautics and Astronautics Journal **15**, 794-803 (1977).

[2] M. Roger, and H. Arbey, "Champ de pression dans un conduit annulaire en présence d'un écoulement tournant de rotation solide" ("Pressure field in a fluid in solid body rotation"), Revue d'Acoustique **16**, 240-242 (1983).

[3] M. Roger, and H. Arbey, "Relation de dispersion des ondes de pression dans un écoulement tournant" ("Dispersion relation of pressure waves in a swirling flow"), Acustica **59**, 95-101 (1985).

[4] V. Golubev, and H. M. Atassi, "Acoustic-vorticity waves in swirling flows," Journal of Sound and Vibration **209**, 203-222 (1998).

[5] C. K. W. Tam, and L. Auriault, "The wave modes in ducted swirling flows", Journal of Fluid Mechanics **371**, 1-20 (1998).

[6] J. Cooper, and N. Peake, "Propagation of unsteady disturbances in a slowly varying duct with mean swirling flow," Journal of Fluid Mechanics **445**, 207-234 (2001).

[7] H. Galbrun, *Propagation d'Une Onde Sonore Dans l'Atmosphère et Théorie des Zones de Silence (Propagation of an acoustic wave in the atmosphere and theory of zones of silence)* (Gauthier-Villars, Paris, 1931).

[8] O. A. Godin, "Reciprocity and energy theorems for waves in a compressible inhomogeneous moving fluid," Wave Motion **25**, 143-167 (1997).

[9] Poiree, "Les équations de l'acoustique linéaire et non linéaire dans un écoulement de fluide parfait" ("Equations of linear and non linear acoustics in a perfect fluid flow"), Acustica **57**, 5-25 (1985).

[10] Peyret, and G. Elias, "Finite-element method to study harmonic aeroacoustics problems," Journal of the Acoustical Society of America **110**, 661-668 (2001).

[11] M. K. Myers, "On the acoustic boundary condition in the presence of flow," Journal of Sound and Vibration **71**, 429-434 (1980).

[12] B. Poirée, "Petites perturbations d'un écoulement tournant" ("Small perturbations in a rotating flow"), Acustica **59**, 85-94 (1985).

[13] S. W. Rienstra, "Sound transmission in slowly varying circular and annular lined ducts with flow," Journal of Fluid Mechanics **380**, 279-296 (1999).

[14] L. Abrahamson, "A finite element algorithm for sound propagation in axisymmetric ducts containing compressible mean flow," AIAA 4th Aeroacoustics Conference, Atlanta (1977).

[15] R. J. Astley, and W. Eversman, "Acoustic transmission in non-uniform ducts with mean flow, part II: the finite element method," Journal of Sound and Vibration **74**, 103-121 (1981).

[16] R. J. Astley, and W. Eversman, "A finite element formulation of the eigenvalue problem in lined ducts with flow," Journal of Sound and. Vibration **65**, 61-74 (1979).

[17] S. Bonnet-Ben Dhia, G. Legendre, and E. Luneville, "Analyse mathématique de l'équation de Galbrun en écoulement uniforme" ("Mathematical analysis of

Galbrun's equation with uniform flow"), Comptes-rendus de l'Académie des Sciences Série IIb **329**, 601-606 (2001).

[18] F. Treyssède, G. Gabard, and M. Ben Tahar, "A mixed finite element method for acoustic wave propagation in moving fluids based on an Eulerian-Lagrangian description," Journal of the Acoustical Society of America **113**, 705-716 (2003).

[19] G. Gabard, F. Treyssède, and M. Ben Tahar, "A numerical method for vibro-acoustic problems with sheared mean flows", accepted in the Journal of Sound and Vibration.

[20] A. H. Nayfeh, *Introduction to Perturbation Techniques* (John Wiley & Sons, 1981).

[21] E. J. Hinch, *Perturbation Methods* (Cambridge University Press, 1991).

[22] A; H. Nayfeh, and D. P. Telionis, "Acoustic propagation in ducts with varying cross sections," Journal of the Acoustical Society of America **54**, 1654-1661 (1973).

[23] M. Ben Tahar, and E. Goy, "Resolution of a vibroacoustic problem in the presence of a nonuniform mean flow," Fourth AIAA Joint Aeroacoustics Conference Paper No. 98-2215 (1998).

[24] K. J. Bathe, *Finite Element Procedures* (Prentice Hall, Englewood Cliffs, 1996).

[25] S. W. Rienstra, and W. Eversman, "A numerical comparison between the multiple-scales and finite-element solution for sound propagation in lined flow ducts," Journal of Fluid Mechanics **437**, 367-384 (2001).

[26] W. Eversman, "A reverse flow theorem and acoustic reciprocity in compressible potential flows in ducts," Journal of Sound and Vibration **246**, 71-95 (2001).

[27] G. K. Batchelor, *An Introduction To Fluid Dynamics* (Cambridge University Press, 1967).

FIGURE CAPTIONS:

FIG.1: Geometry of a slowly varying duct carrying flow with swirl. The acoustic inlet being located at the top section z=0m, the sketched duct is expanding from the acoustical point of view.

FIG.2: $\lambda/10$ FEM meshes for a duct: (a) slowly contracting at f=300Hz, (b) slowly expanding at f=850Hz.

FIG.3: Mean flow variables calculated from the aerodynamic MS model of Cooper and Peake, with M_0=−0.21 and Ω_0=+0.30 at the acoustic outlet (z=0 section): (a) density, (b) celerity, (c) pressure, (d) azimuthal velocity and (e) axial velocity.

FIG.4: Pressure modulus in Pa of the (−5,1) mode launched in an expanding rigid-wall duct, with M_0=−0.21 and Ω_0=+0.30 at the acoustic outlet (z=0m): (a)-(b)-(c) MS solutions for f=350, 500 and 650Hz respectively, (d)-(e)-(f) FEM solutions.

FIG.5: Pressure modulus in Pa of the (−5,1) mode at f=500Hz (rigid-wall duct, with M_0=−0.21 and Ω_0=+0.30). FEM solution with mesh refinement.

FIG.6: Pressure modulus in Pa of the (+20,0) mode launched in a contracting rigid-wall duct, with M_0=+0.30 and Ω_0=+0.30 at the acoustic outlet (z=0m): (a)-(b)-(c) MS solutions for f=1250, 1500 and 1750Hz respectively, (d)-(e)-(f) FEM solutions.

FIG.7: Axial intensity in W/m^2 (post-processed from FEM solutions) of the (+20,0) mode at: (a) f=1250Hz, (b) f=1500Hz, (c) f=1750Hz.

FIG.8: Pressure modulus in Pa of the (±3,0) mode launched in a contracting lined duct (Z_1=Z_2=408−408i), with M_0=+0.52 and Ω_0=+0.20 at the acoustic outlet (z=0m): (a)-(b) MS solutions at 200Hz for m=−3 and m=+3, (c)-(d) respective FEM solutions, (e)-(f) MS solutions at 300Hz for m=−3 and m=+3, (g)-(h) respective FEM solutions.

FIG.9: Pressure modulus in Pa of the (±10,1) mode launched in an expanding lined duct (Z_1=Z_2=1020−1020i) at 850Hz, with M_0=−0.35 and Ω_0=+0.20 at the acoustic outlet (z=0m): (a)-(b)-(c) MS solutions for m=−10, m=10 with no swirl, and m=+10 respectively, (d)-(e)-(f) FEM solutions.

FIG.10: Axial intensity in W/m^2 (computed from FEM solutions) of the (±10,1) mode at f=850Hz for: (a) m=−10, (b) m=10 with no swirl, (c) m=+10. Enlargements of intensity vectors are also shown at walls.

FIG.1

Fabien Treyssède

JASA

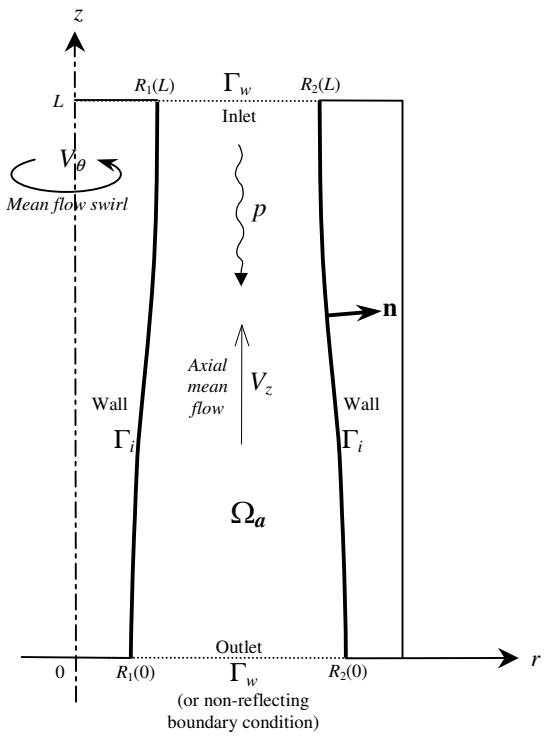

FIG.2

Fabien Treyssède

JASA

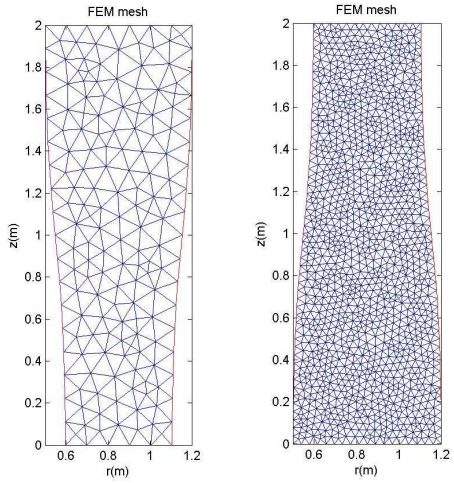

(a) (b)

FIG.3

Fabien Treyssède

JASA

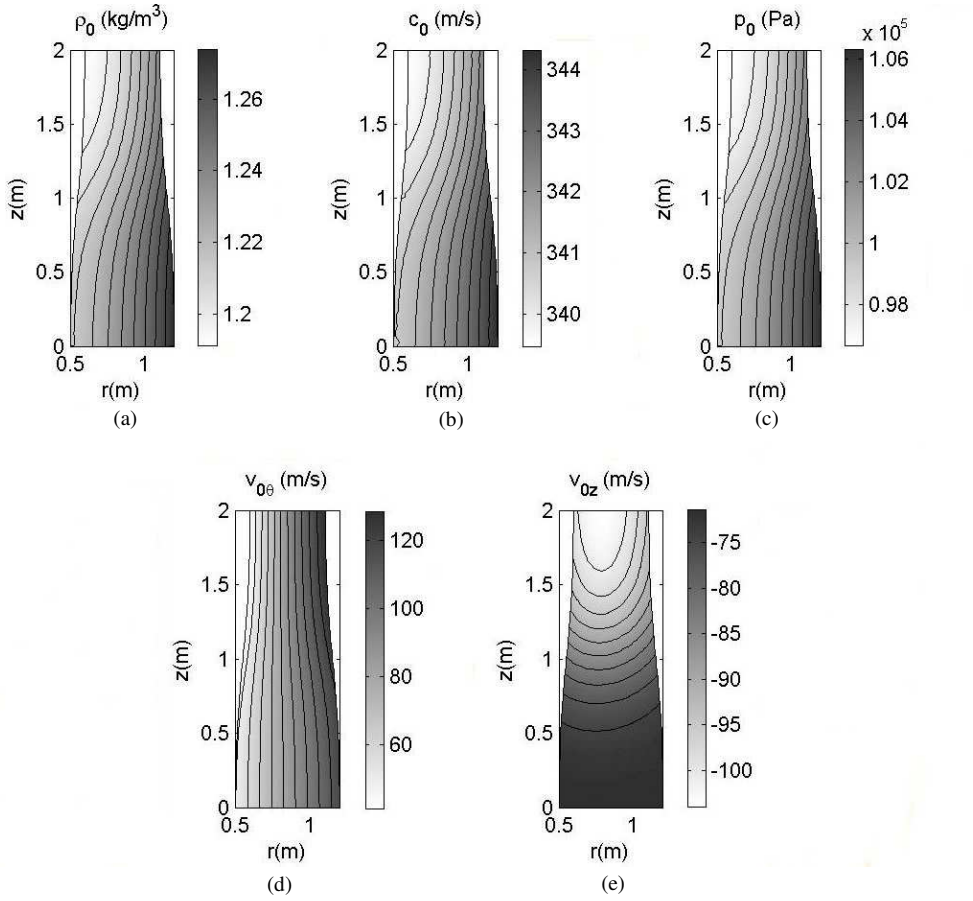

FIG.4

Fabien Treyssède

JASA

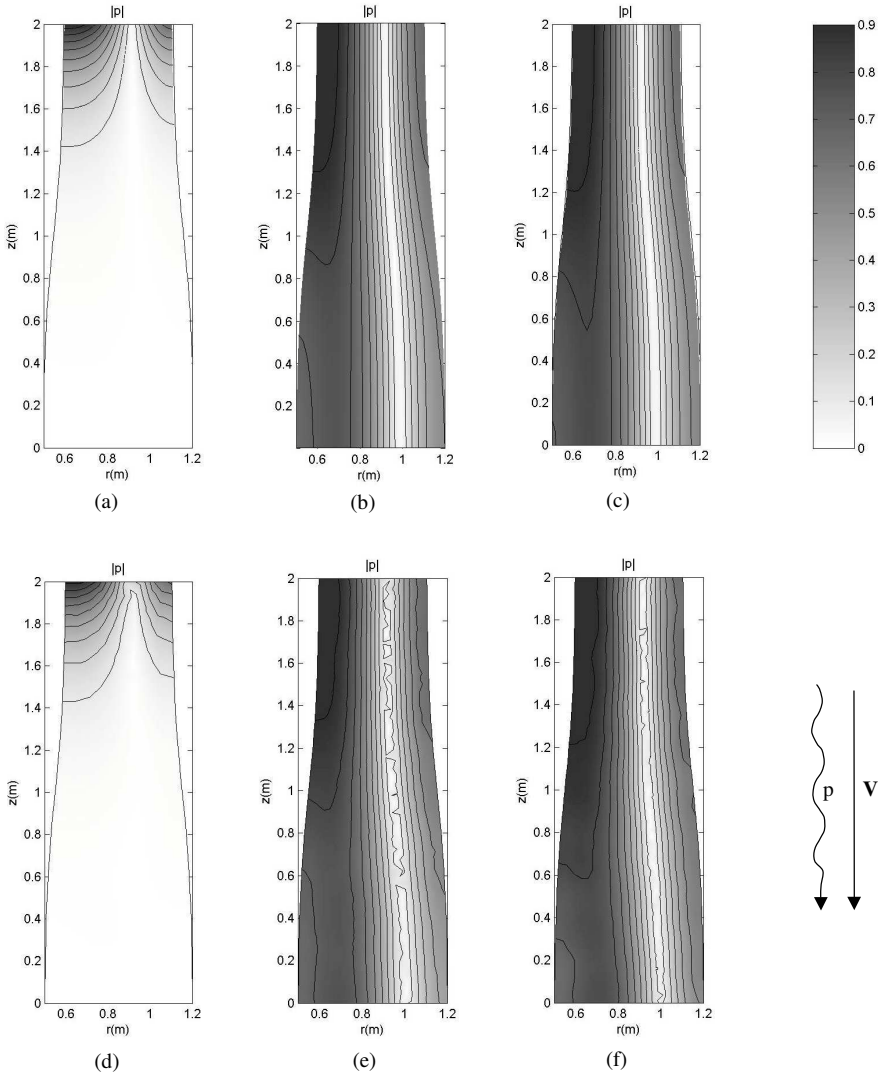

FIG.5

Fabien Treyssède

JASA

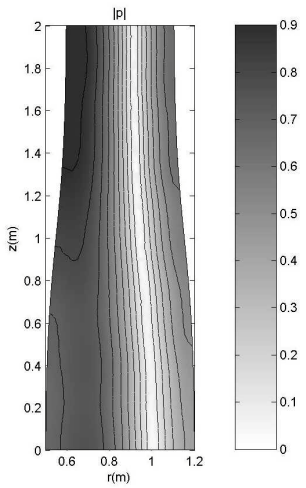

FIG.6

Fabien Treyssède

JASA

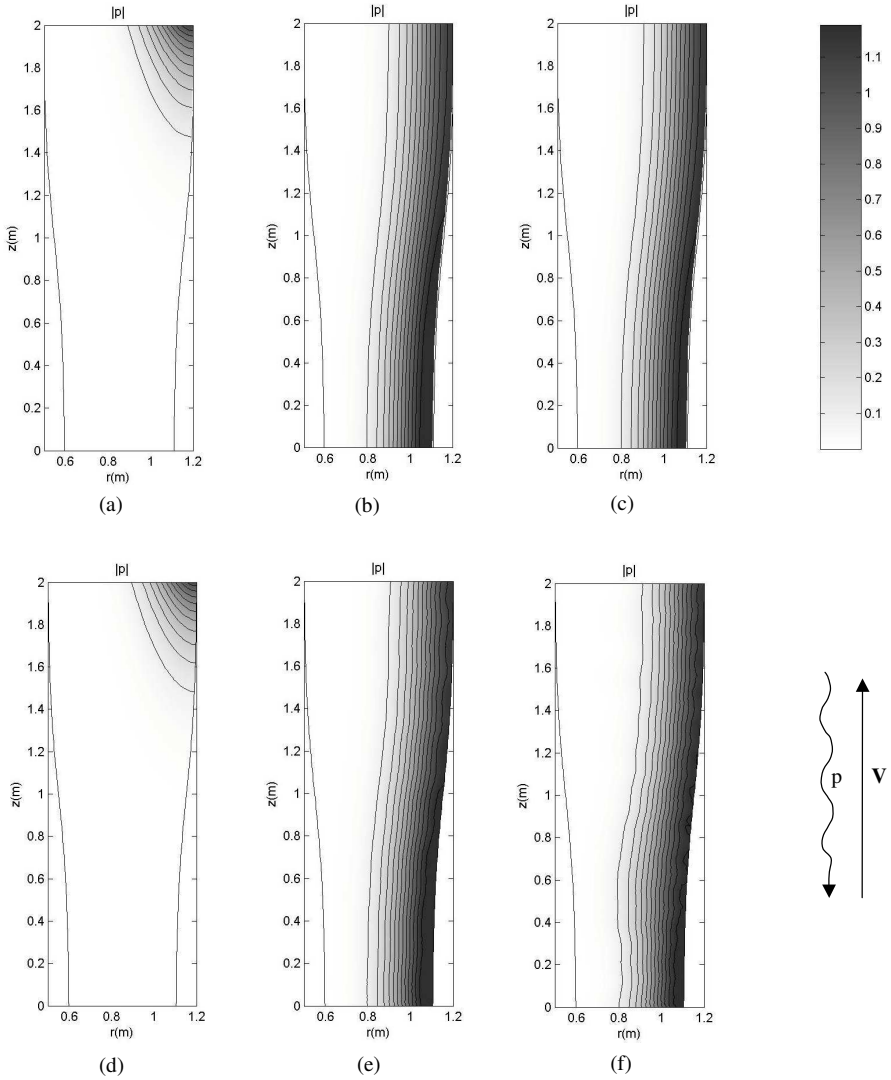

FIG.7

Fabien Treyssède

JASA

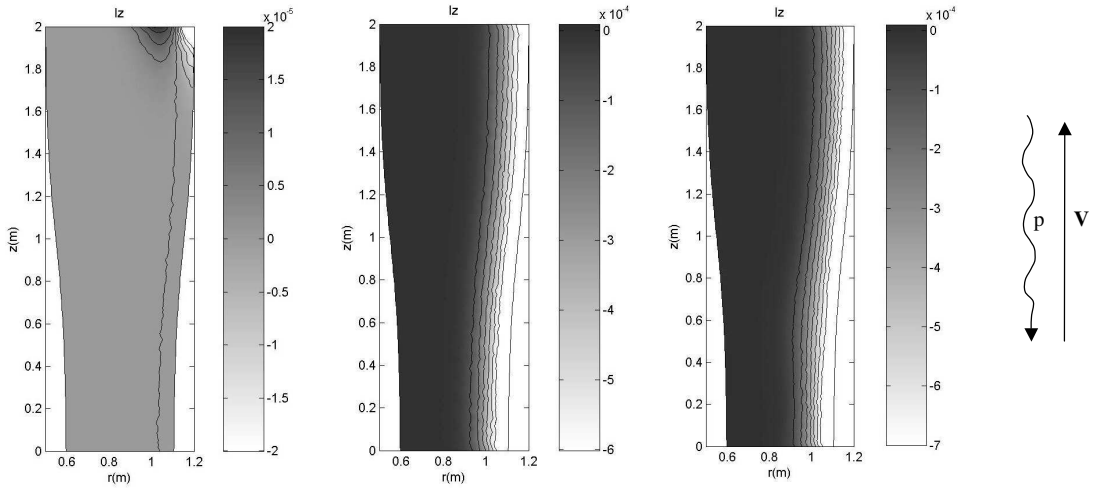

FIG.8

Fabien Treyssède

JASA

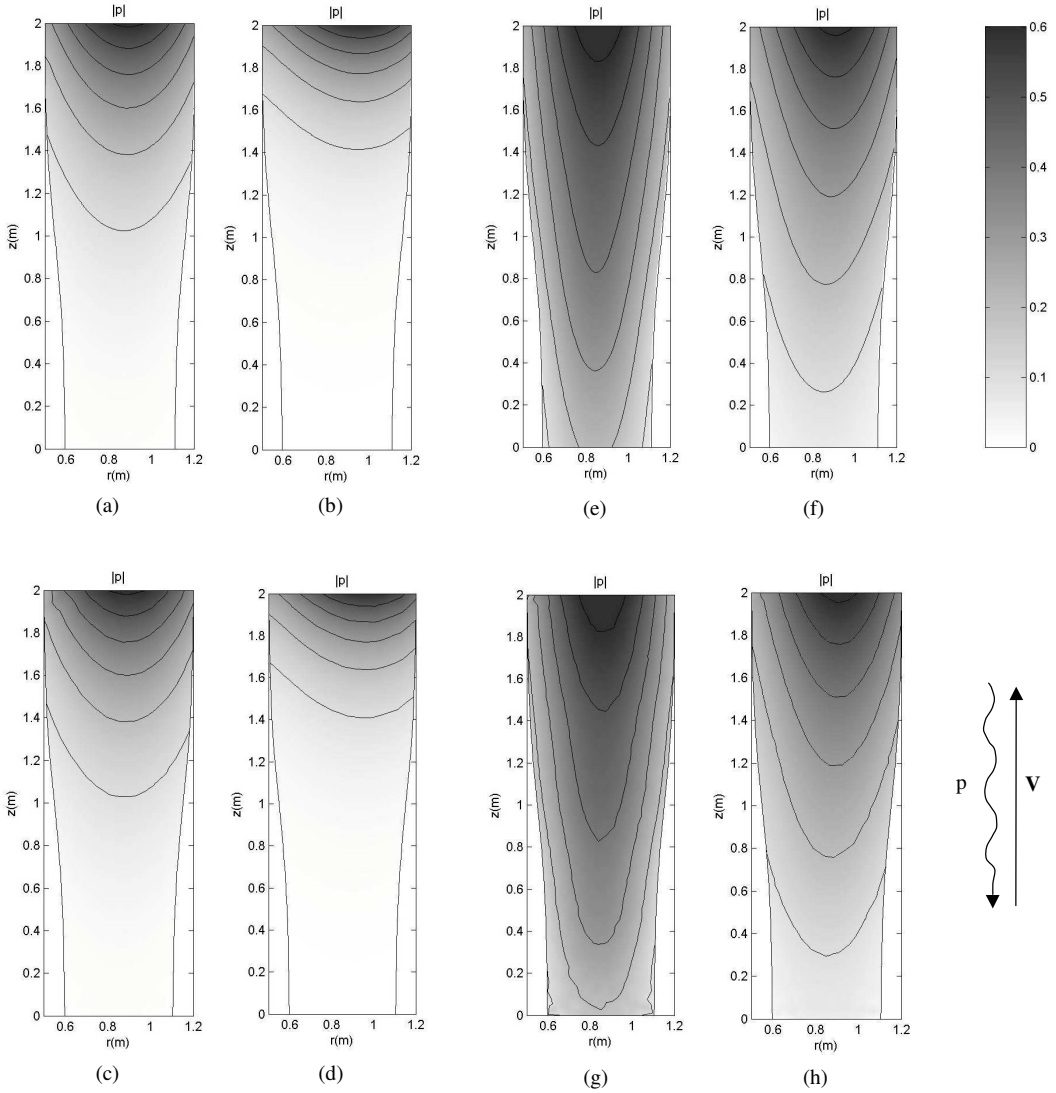

FIG.9

Fabien Treyssède

JASA

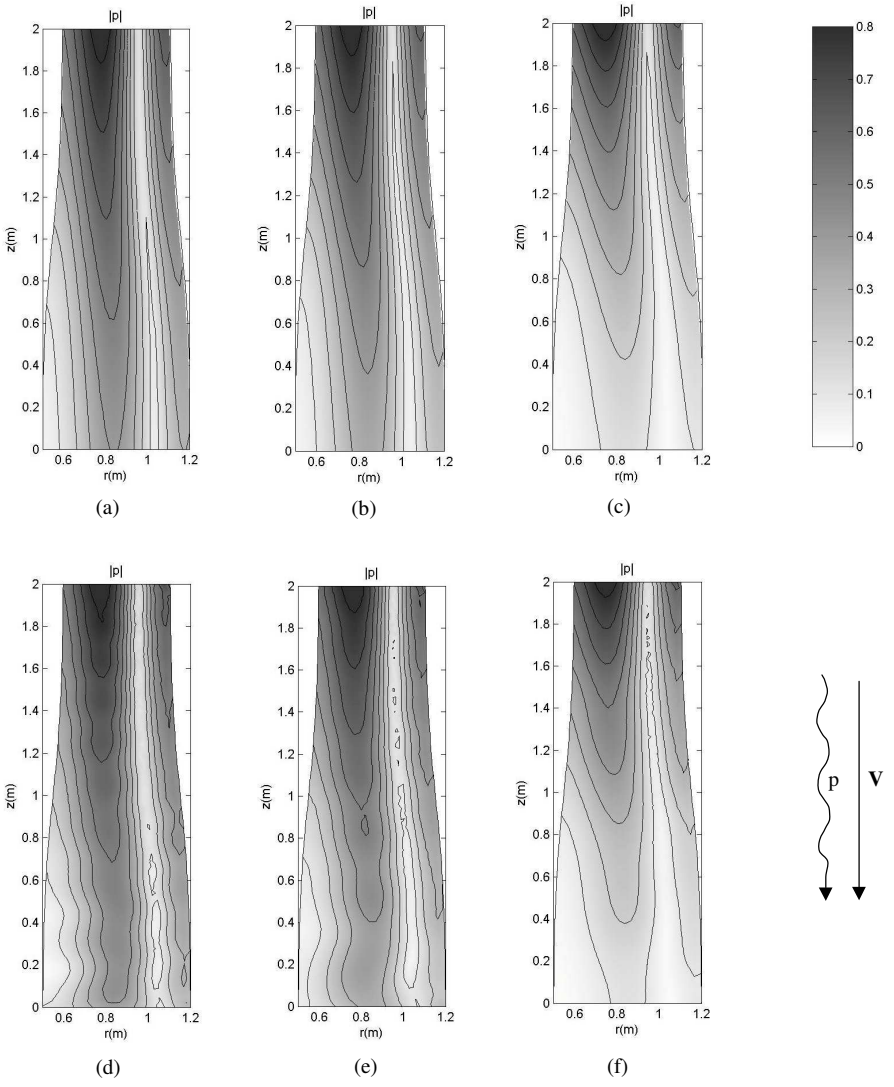

FIG.10

Fabien Treyssède

JASA